ISSN 0915-633X

NATIONAL INSTITUTE FOR FUSION SCIENCE

Transport Coefficients of InSb in a Strong Magnetic Field

H. Nakamura, K. Ikeda and S. Yamaguchi

(Received - Oct. 3, 1997)

NIFS-540 Feb. 1998

RESEARCH REPORT
NIFS Series

NAGOYA, JAPAN

Transport Coefficients of InSb in a Strong Magnetic Field

Hiroaki Nakamura, Kazuaki IKEDA[a], and Satarou Yamaguchi

National Institute for Fusion Science (NIFS),

[a] *Department of Fusion Science, The Graduate University for Advanced Studies,*

Oroshi-Cho, Toki-City, Gifu-Prefecture, 509-52, Japan,

Phone&Fax : +81-52-789-4538, E-mail:hiroaki@rouge.nifs.ac.jp,

http://rouge.nifs.ac.jp/~hiroaki/index.html

(This paper was presented in the XVI International Conference on Thermoelectrics, Dresden, Germany (1997).)

Abstract

Improvement of a superconducting magnet system makes induction of a strong magnetic field easier. This fact gives us a possibility of energy conversion by the Nernst effect. As the first step to study the Nernst element, we measured the conductivity, the Hall coefficient, the thermoelectric power and the Nernst coefficient of the InSb, which is one of candidates of the Nernst elements. From this experiment, it is concluded that the Nernst coefficient is smaller than the theoretical values. On the other hand, the conductivity, the Hall coefficient ant the thermoelectric power has the values expected by the theory.

Keywords: *indium antimonide, Nernst effect, Nernst coefficient, Nernst element, thermomagnetic conversion, transport coefficient, thermoelectric power, mobility, Boltzmann equation, parabolic band, phonon, scattering process, figure of merit, strong magnetic field*

I. INTRODUCTION

One of the authors, S. Y., proposed [1,2] the direct electric energy conversion of the heat from plasma by the Nernst effect in a fusion reactor, where a strong magnetic field is used to confine a high temperature fusion plasma. He called [1,2] the element which induces the electric field in the presence of temperature gradient and magnetic field, as Nernst element. In his paper [1,2], he also estimated the figure of merit of the Nernst element in a semiconductor model. In his result [1,2], the Nernst element has high performance in low temperature region, that is, 300 - 500 K. Before his works, the Nernst element was studied in the 1960's [3]. In those days, induction of the magnetic field had a lot of loss of energy. This is the reason why the Nernst element cannot be used. Nowadays an improvement on superconducting magnet gives us higher efficiency of the induction of the strong magnetic field. We started a measuring system of transport coefficients in the strong magnetic field to estimate efficiency of the Nernst element on a few years ago [4]. As the first candidate of the Nernst element, we choose InSb, which is expected to have the high figure of merit according to the single-band model [5]. The experimental results show that the Nernst coefficient is smaller than the theoretical values. On the other hand, the conductivity, the Hall coefficient and the thermoelectric power has the values expected by the theory. In this paper, we introduce the experimental results and compare the theoretical calculations.

II. EXPERIMENT

A. Choice of material

We discuss the principle of transport phenomena in a magnetic field and a temperature gradient. This behavior is written by two phenomenological equations [6] as follows:

$$\boldsymbol{E} = \frac{\boldsymbol{J}}{\sigma} + \alpha \cdot \boldsymbol{\nabla} T + R_{\rm H} \boldsymbol{B} \cdot \boldsymbol{J}, \tag{1}$$

$$\boldsymbol{q} = \alpha T \boldsymbol{J} - \kappa \boldsymbol{\nabla} T + N T \boldsymbol{B} \times \boldsymbol{J} + L \boldsymbol{B} \times \boldsymbol{\nabla} T, \tag{2}$$

where $\boldsymbol{E}$ is electrical field, $\boldsymbol{J}$ current density, $\boldsymbol{B}$ magnetic field, T temperature, σ electrical conductivity, α thermoelectric power, $R_{\rm H}$ Hall coefficient, N Nernst coefficient, κ thermal conductivity and L Righi-Leduc coefficient.

To simplify the discussion of the efficiency, we replace all transport coefficients by averaged quantities, which do not depend on position within a device. In order to estimate efficiency of the Nernst element, it is useful to define the figure of merit $Z_{\rm N}$ as follows [3]:

$$Z_{\rm N} \equiv \frac{\sigma B^2 N^2}{\kappa}. \tag{3}$$

Using eq.(1), the optimal efficiency of thermomagnetic generators $\varepsilon_{\rm N}$ is given by [3]

$$\varepsilon_{\rm N} = \varepsilon_{\rm C} \left(\frac{1 - \delta_{\rm N}^*}{1 + \frac{T_{\rm low}}{T_{\rm high}} \delta_{\rm N}^*} \right), \tag{4}$$

where $T_{\rm high}(T_{\rm low})$ is the temperatures of the heating (cooling) block, $\varepsilon_{\rm C}$ the carnot efficiency, $(T_{\rm high} - T_{\rm low})/T_{\rm high}$, and

$$\delta_{\rm N}^* = \sqrt{1 - Z_{\rm N} \left(\frac{T_{\rm low} + T_{\rm high}}{2} \right)}. \tag{5}$$

The value of $\delta_{\rm N}^*$ must be a real number. This fact impose the following restriction as [3]:

$$Z_{\rm N} \left(\frac{T_{\rm low} + T_{\rm high}}{2} \right) \leq 1. \tag{6}$$

We plot the normalized efficiency, $\varepsilon_{\rm N}/\varepsilon_{\rm C}$ in Fig. 1 as a function of the figure of merit. This figure shows that $\varepsilon_{\rm N}$ increases monotonously as $Z_{\rm N}$ becomes larger. We, therefore, must choose the high-$Z_{\rm N}$ materials. We consider the transport coefficients to choose them. It is known from the Boltzmann equation that both conductivity and Nernst coefficient are proportional to Hall mobility [7,8]. This fact derives the form [1,4]:

$$Z_N \propto \mu^3. \tag{7}$$

The equation (7) is a criterion for searching the Nernst element. Under this criterion, we first propose indium antimonide, InSb as a candidate of the Nernst element. To compare the mobility of InSb with the other materials, we summarize the values of the mobilities in Table I.

B. Measurement of transport coefficients and results

1. Conductivity and Hall coefficient

The carrier concentration of the InSb crystals investigated is 6.6×10^{20} [m^{-3}] and its mobility 21 [m^2/V/s] at 77K. This sample exhibited intrinsic behavior near room temperature. Copper wires with 50 μm-diameter are spark-bonded onto a crystal by using a capacitor discharge. Chromel-Alumel thermocouples, 0.5 mm in diameter, are contact to heating and cooling units with silver epoxy. The temperature of the sample is controlled within 270-370K by the heat bath, the water temperature of which is kept a constant. We induced a strong magnetic field up to 4 Tesla by the superconducting coil to measure magnetoresistance of the sample. Analog signals of the thermocouples and voltage source are amplified and converted to digital data. The personal computer acquires these data and draws figures in real time. We use the van der Pauw method [9] to measure the conductivity and Hall coefficients. A geometry for the van der Pauw method is shown in Fig. 2. Figure 3(a) shows the temperature dependence of the resistivity at B=0 Tesla. The temperature dependence of the Hall coefficient is represented in Fig. 3(b).

2. Thermoelectric power and Nernst coefficient

The sample of measurement of the thermoelectric power and the Nernst element is the same material as the van der Pauw method. However, the shape of the sam-

ple is changed from the square to the bridged shape (Fig. 4). In order to make temperature gradient in the sample, we used thermofoil heater for a heating copper block side, the water temperature of which is controlled by a low temperature incubator, for a cooling one. Using the heating and cooling units, the thermal difference across the sample was within 10-100K. The thermoelectric voltage, V_α and the Nernst one, V_N have the following relations between the thermoelectric power and the temperature gradient as

$$V_\alpha = L\alpha|\nabla\ T| \approx \alpha\Delta T, \tag{8}$$

$$V_N = wNB|\nabla\ T| \approx \frac{wNB\Delta T}{L}, \tag{9}$$

where ΔT is $(T_{\rm high} - T_{\rm low})$, w the width of the sample and L the length defined by Fig. 4. Here we define the following physical quantity, β to compare the thermoelectric power and the Nernst effect:

$$\beta \equiv NB, \tag{10}$$

which has the same dimension, [V/K] as α. The results of the measurement of α and β in Figs. 5–6. The thermoelectric power doesn't change very much as the magnetic field is induced. On the other hand, the β depends on the magnetic field very much. In Fig. 6(a), we plot the results as the crosses and the theoretical values as the filled circles. The theoretical values are explained in the later. The difference between the experimental results and the theoretical ones is the order of 10. For the strong magnetic field, the results are shown in Fig. 6(b).

III. ANALYSIS AND PHYSICAL QUANTITIES

A. Carrier concentration

In the weak field limit, the Hall coefficient and the carrier concentration has the form [8]

$$R_{\rm H} = \frac{3\pi}{8|e|}\frac{p - nb^2}{(p+nb)^2} \approx -\frac{3\pi}{8|e|n}, \tag{11}$$

where we define $b = \mu_{\rm n}/\mu_{\rm p}$ and the hole parts are neglected because $b \approx 100$ for InSb [10,11]. Equation (11) and Fig. 3(b) gives the carrier concentration of the electron in Fig. 7. We can fit the following function of the temperature by the least square method as

$$n(T) = 3.3 \times 10^{20} T^{1.5} \exp\left(-\frac{2600}{kT}\right). \tag{12}$$

We assume that the sample is in the intrinsic region near room temperature. The carrier concentration of the intrinsic semiconductor is written by [8]

$$n_{\rm i}(T) = 2\left(\frac{\sqrt{m_{\rm n} m_{\rm p}} kT}{2\pi\hbar^2}\right)^{\frac{3}{2}} \exp\left(-\frac{E_{\rm G}}{2kT}\right), \tag{13}$$

where $E_{\rm G}$ is the energy gap, $m_{\rm n}$ the effective mass of the electron, and $m_{\rm p}$ the effective mass of the hole. Comparing eq. (12) with eq. (13), we obtain

$$E_{\rm G} \approx 2600 \times \frac{k}{|e|} = 0.22 \text{ [eV]}, \tag{14}$$

$$m_{\rm n} m_{\rm p} \approx \left\{\left(\frac{3.3 \times 10^{20}}{2}\right)^{2/3} \frac{2\pi\hbar^2}{k}\right\}^2 \approx 1.7 \times 10^{-2} m_0^2. \tag{15}$$

B. Mobility of electron

In the weak field limit, the Boltzmann equation for the single parabolic non-degenerated band model gives the conductivity as follows [8]:

$$\sigma = 1/\rho = |e| n \mu_{\rm n}\left(1 + \frac{p}{nb}\right) \approx |e| n \mu_{\rm n}, \tag{16}$$

where we use $b \ll 1$ for InSb. Equations (11) and (16) give the mobility of the electron in Fig. 8. The temperature dependence of the mobility of the electron is obtained as

$$\mu_{\rm n} \approx 7.5 \times \left(\frac{T}{300}\right)^{-1.50} [\text{m}^2/\text{V/s}]. \tag{17}$$

The exponent -1.5 denotes that the dominant scattering process is acoustic phonon scattering.

C. Mobility of hole

In the strong magnetic field limit, the Nernst coefficient of the intrinsic semiconductor becomes [10]

$$N \approx \frac{k}{|e|}\mu_{\rm p}\left(4+\frac{E_{\rm G}}{kT}\right). \tag{18}$$

Substituting the values of the Nernst coefficient given by the experiment at $B = 4$ Tesla in the eq. (18), we obtain the mobility of the hole in Fig. 9. By the least square method, we also have the temperature dependence of the hole mobility as

$$\mu_{\rm p}(B = 4{\rm Tesla}) \approx 0.065 \times \left(\frac{T}{300}\right)^{-1.7} [{\rm m}^2/{\rm V/s}]. \tag{19}$$

D. Fermi level

The thermoelectric power gives the Fermi level as follows [8]:

$$\begin{aligned}\alpha &= \alpha_{\rm n}\frac{\sigma_{\rm n}}{\sigma_{\rm n}+\sigma_{\rm p}} + \alpha_{\rm p}\frac{\sigma_{\rm p}}{\sigma_{\rm n}+\sigma_{\rm p}} \\ &= \alpha_{\rm n}\left(\frac{1}{1+\frac{p}{nb}}\right) + \alpha_{\rm p}\left(\frac{\frac{p}{nb}}{1+\frac{p}{nb}}\right) \\ &\approx \alpha_{\rm n} = -\frac{k}{|e|}\left(2-\frac{\zeta_{\rm n}}{kT}\right),\end{aligned} \tag{20}$$

where is the Fermi level from the edge of the conduction band and negative. Equation (20) and the experimental results of the thermoelectric power give the Fermi level in Fig. 10. In the intrinsic region, the Fermi level becomes [8]

$$\zeta_{\rm n} = -\frac{E_{\rm G}}{2} + \frac{3kT}{4|e|}\ln\left(\frac{m_{\rm p}}{m_{\rm n}}\right) \quad [{\rm eV}]. \tag{21}$$

Analysis in Fig. 10 gives the temperature dependence of the Fermi level as follows

$$\zeta_{\rm n} = -0.117 + 3.2\frac{kT}{|e|} \quad [{\rm eV}]. \tag{22}$$

From eqs. (21) and (22), the energy gap and the ratio of the effective masses of the electron and the hole is given as

$$E_{\rm G} \approx 0.23 \quad [\ {\rm eV}\ ], \quad \frac{m_{\rm p}}{m_{\rm n}} \approx 73. \tag{23}$$

IV. DISCUSSION AND CONCLUSIONS

We summarize basic physical quantities obtained by the experiment in Table II, where the reference values are also written. This table shows that the experimental results are almost consistent with the previous works. It is concluded that the Hall coefficient, the conductivity and the thermoelectric power of InSb near room temperature in the weak field are given by the Boltzmann equation for the non-degenerate parabolic two-band with the acoustic phonon scattering. However, the Nernst coefficient is very smaller than the theoretical value in the weak field. The behavior of the Nernst coefficient in the strong magnetic field is consistent with the two-band model. We try to explain the difference between the experimental and the theoretical values of the Nernst coefficient in the weak field. Moreover we will measure the thermal conductivity in the magnetic field to estimate the figure of merit.

ACKNOWLEDGMENTS

The authors are grateful to Dr. Tatsumi in Sumitomo Electric Industries and Prof. Kuroda in Nagoya university for providing semiconductors. We appreciate Prof. Motojima and Prof. Iiyoshi in the National Institute for Fusion Science for their helpful comments.

REFERENCES

[1] S. Yamaguchi, A. Iiyoshi, O. Motojima, M. Okamoto, S. Sudo, M. Ohnishi, M. Onozuka and C. Uesono, *"Direct Energy Conversion of Radiation Energy in Fusion Energy, Proc. of 7th Int. Conf. Merging Nucl. Energy Systems"*, *Proc. of 7th Int. Conf. Merging Nucl. Energy Systems* (ICENES)", (1994) 502.

[2] S. Yamaguchi, K. Ikeda, H. Nakamura and K. Kuroda, *"A Nuclear Fusion Study of Thermoelectric Conversion in Magnetic field"*, *4th Int. Sympo. on Fusion Nuclear Tech.*, ND-P25, Tokyo, Japan, April (1997).

[3] T. C. Harman and J. M. Honig, *"Thermoelectric and Thermomagnetic Effects and Applications"*, McGraw-Hill Book Company, (1967), Chap. 7, p. 311.

[4] K. Ikeda, H. Nakamura, S. Yamaguchi and K. Kuroda, "Measurement of Transport properties of Thermoelectric Materials in the Magnetic Field", J. Adv. Sci., **8**, (1996) 147, (in Japanese).

[5] H. Nakamura, K. Ikeda, S. Yamaguchi and K. Kuroda, "Transport Coefficients of Thermoelectric Semiconductor InSb", J. Adv. Sci., **8**, (1996) 153, (in Japanese).

[6] L. D. Landau, E. M. Lifshitz and L. P. Petaevskii, *"Electrodynamics of Continuous Media"*, 2nd Edition, Pergamon Press, (1984)101.

[7] E. H. Putly, *"The Hall Effect and Related Phenomena"*, London, Butterworth &Co. Ltd., (1960), Chap. 3, p. 66.

[8] K. Seeger, *"Semiconductor Physics"*, Springer-Verlag, (1989).

[9] L. J. van der Pauw, "A Method of Measuring Specific Resistivity and Hall Effect of Discs of arbitrary Shape", Philips Res. Rep., **13**, (1958) 1.

[10] G. Madelung, *"Physics of III-V Compounds"*, J. Wiley & Sons, (1964) 115.

[11] J. D. Wiley, *"Semiconductors and Semimetals"*, Vol. 10, ed. by R. K. Willardson and A.C. Beer, Academic Press, (1975) 169.

[12] L. Sosnowski, *"Thermo-Electric and Thermo-Magnetic Effects", Proc. Int'l School of Physics "Enrico Fermi" XXII, Semiconductors*, (Academic Press, New York and London 1963) 436.

[13] H. J. Hrostowski, F. J. Morin, T. H. Geballe, and G. H. Wheatley, Phys. Rev., **100**, (1955) 1672.

[14] D. M. Zengin, J. Phys., **D16**, (1983) 635.

[15] D. M. S. Bagguley, M. L. A. Pobinson and R. A. Strandling, Phys. Lett., **6**, (1963) 143.

InSb	7.7	[m^2 / V sec]
HgSe	2.0	
HgTe	2.5	
InAs	3.3	

TABLE I. Mobilities of electron near room temperature.

physical quantity	experimental result	reference value
carrier concentration [m-3]	$3.3\times10^{20}T^{1.5}\exp\left(-\frac{0.22[eV]}{kT}\right)$	$6\times10^{20}T^{3/2}\exp\left(-\frac{0.26[eV]}{2kT}\right)$
effective mass	$m_n\, m_p = 17\times10^{-2}\, m_e^2$	$m_n = 0.01359\, m_e$
	$\frac{m_p}{m_n} \approx 73$	$m_p = 0.45\, m_e$
mobility * [m^2/V/s]		
electron	$7.5\times\left(\frac{T}{300}\right)^{-1.50}$	$7.7\left(\frac{T}{300}\right)^{-1.66}$
hole	$0.065\times\left(\frac{T}{300}\right)^{-1.7}$	$0.085\left(\frac{T}{300}\right)^{-2}$
	at B = 4 Tesla	at B = 0 Tesla
Fermi level	$\zeta_n = -0.117 + 3.2\frac{kT}{e}$ [eV]	----------

TABLE II. Comparison of the experimental results and the theoretical vales.

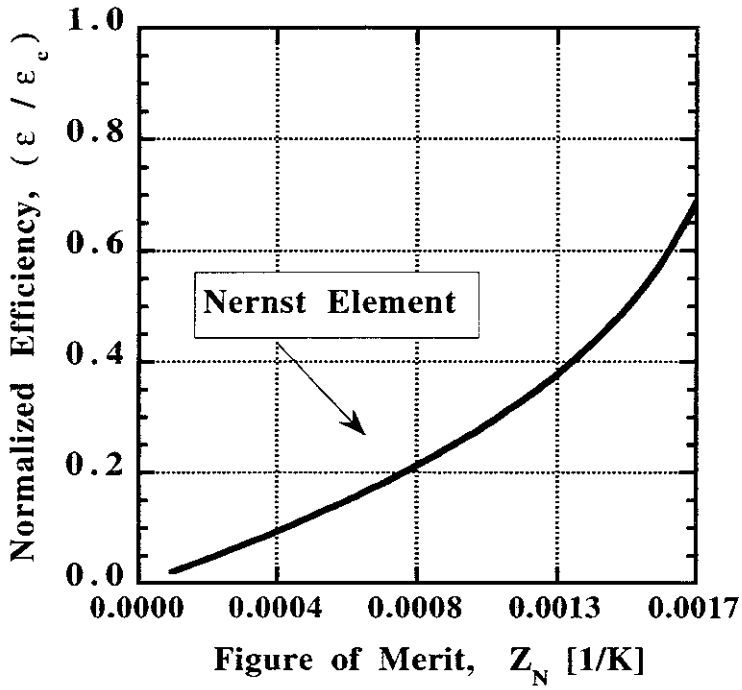

FIG. 1. The maximum efficiency of the Nernst element as a function of Z_{N}.

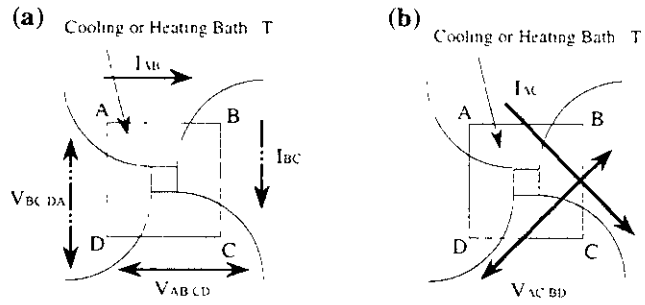

FIG. 2. Sample geometries for performing (a) resistivity and (b) Hall measurements by the van der Pauw method. Size of sample is 4mm × 4mm × 1mm.

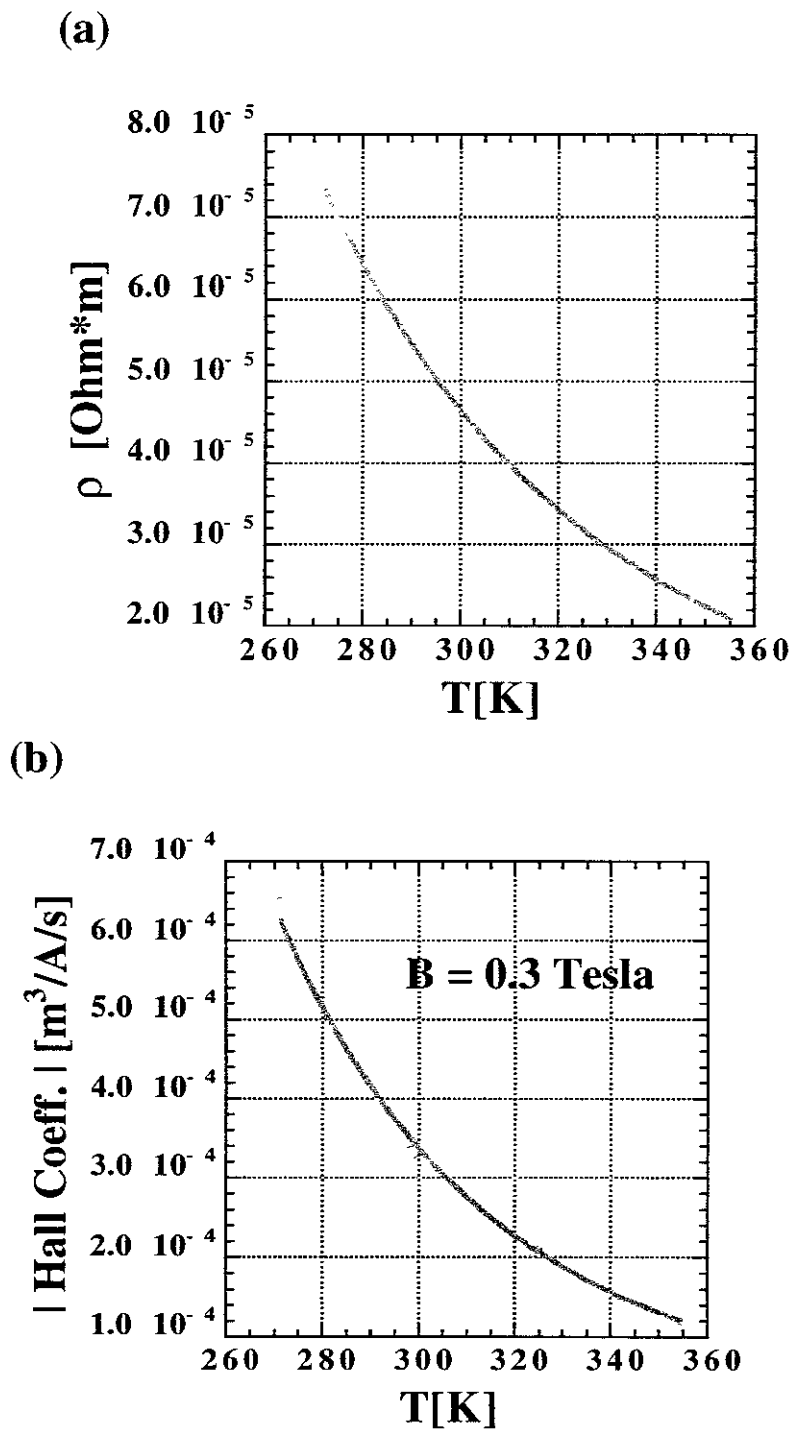

FIG. 3. Resistivity (a) and Hall coefficient (b) of InSb sample as a function of temperature. The closed circles indicate the experimental results. The solid curve is a guide of eyes.

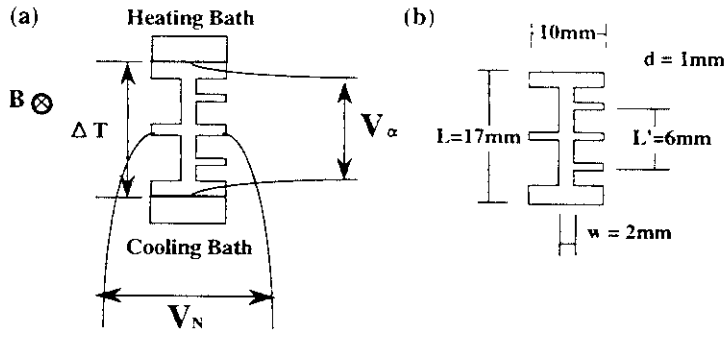

FIG. 4. Shape of the sample for measuring the thermoelectric power and the Nernst effect. This shape is called the "bridged shape".

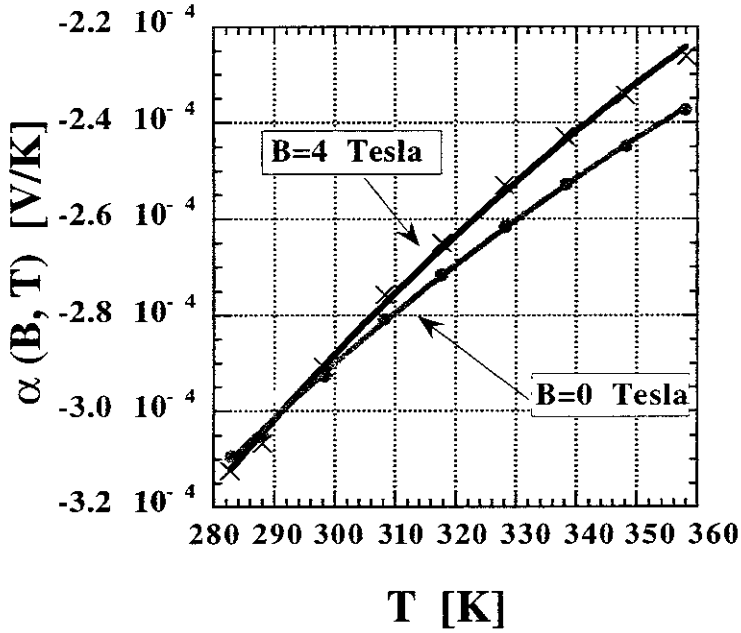

FIG. 5. Thermoelectric power of InSb sample as a function of temperature. The crosses represent experimental results at $B = 0$ Tesla. The filled circles indicate the experimental results at $B = 4$ Tesla. The solid curves are guide for eyes.

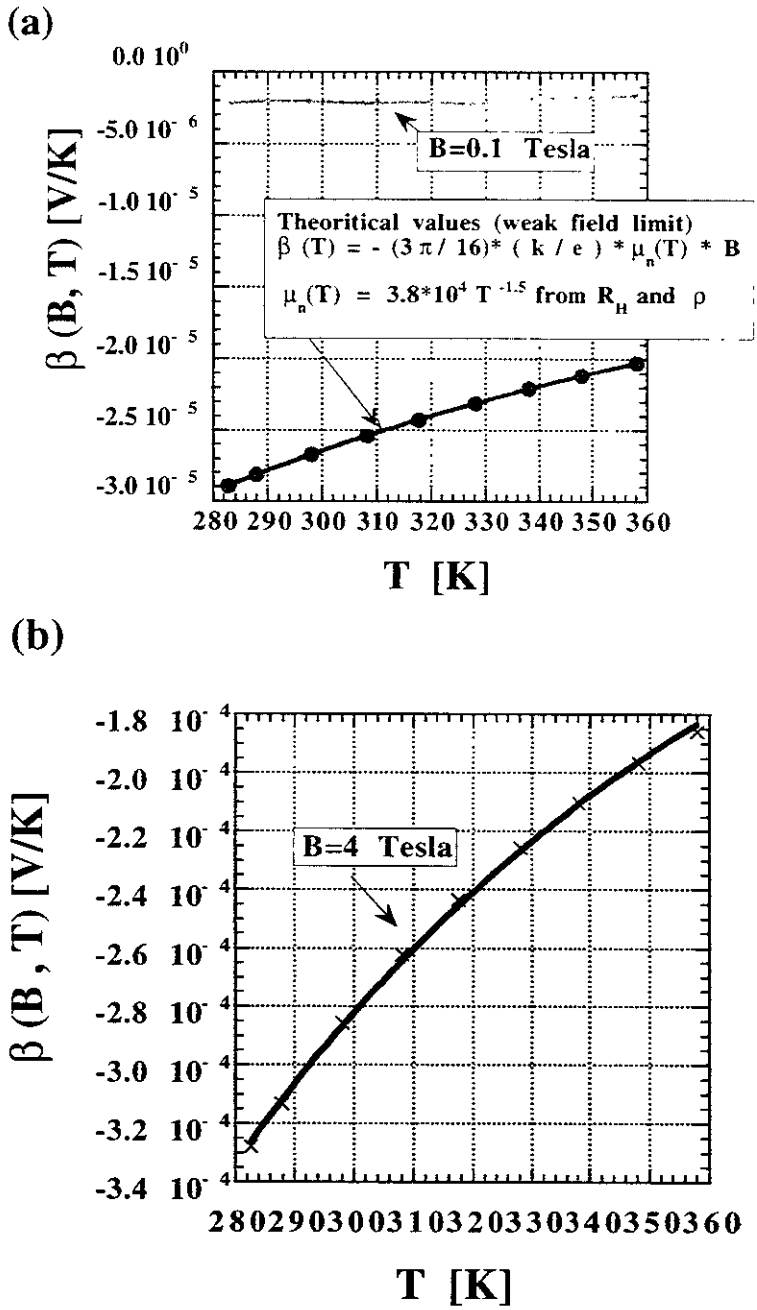

FIG. 6. Plot of Nernst effects, $\beta = N \times B$ in the case of $B = 0.1$ Tesla (a) and 4 Tesla (b). The crosses indicate the experimental results. The filled circles in Fig. 6(a) were calculated by the single band model with the mobilities which were given from the Hall coefficients and resistivities. In Fig. 6(b), the solid curve is given by the least square method.

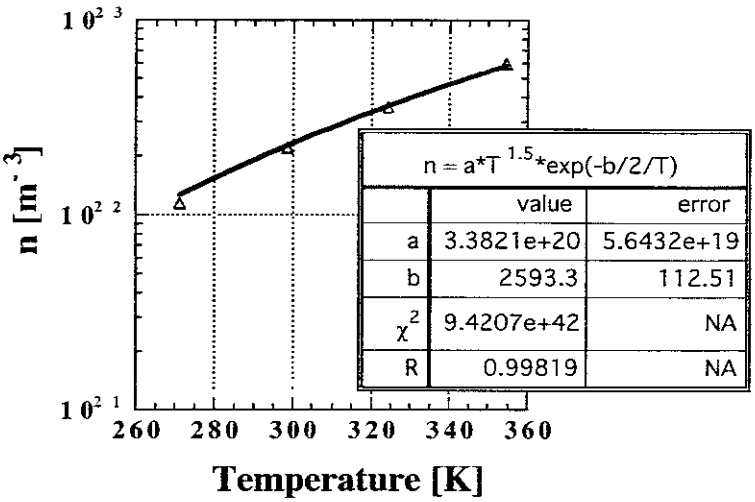

FIG. 7. Temperature dependence of the carrier concentration of the electron. Fitting function is $n(T) = 3.3 \times 10^{20} T^{1.5} \exp\left(-\frac{2600}{kT}\right)$. Comparing the intrinsic concentration eq. (13), we have $E_{\mathrm{G}} \approx 0.22$ [eV] and $m_{\mathrm{n}} m_{\mathrm{p}} \approx 1.7 \times 10^{-2} m_0^2$.

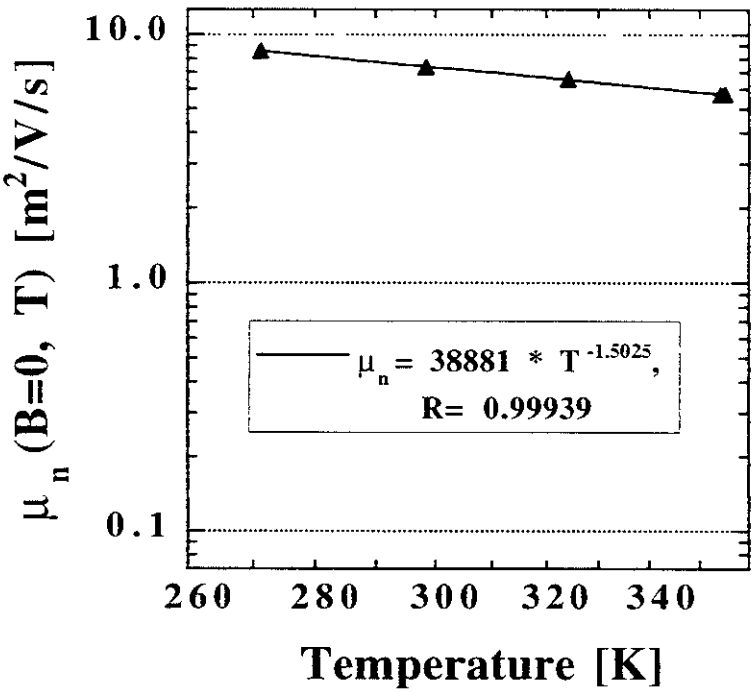

FIG. 8. Temperature dependence of the electron mobility. The experimental results are fitted by $\mu_{\rm n} \approx 7.5 \times (T/300)^{-1.50}$ [$\rm m^2/V/s$].

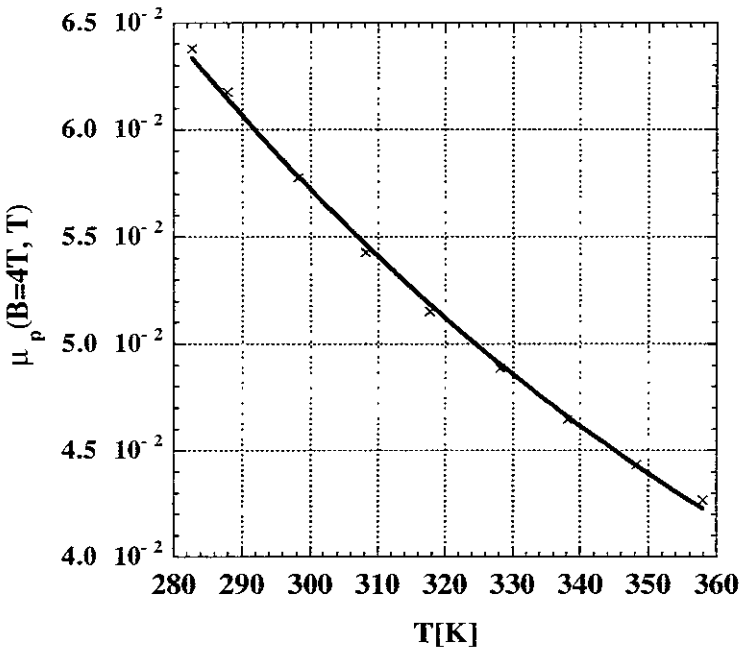

FIG. 9. Temperature dependence of the hole mobility from the Nernst coefficients. The experimental results are fitted by $\mu_{\rm p}(B = 4{\rm Tesla}) \approx 0.065 \times (T/300)^{-1.7}$ [$\rm m^2/V/s$].

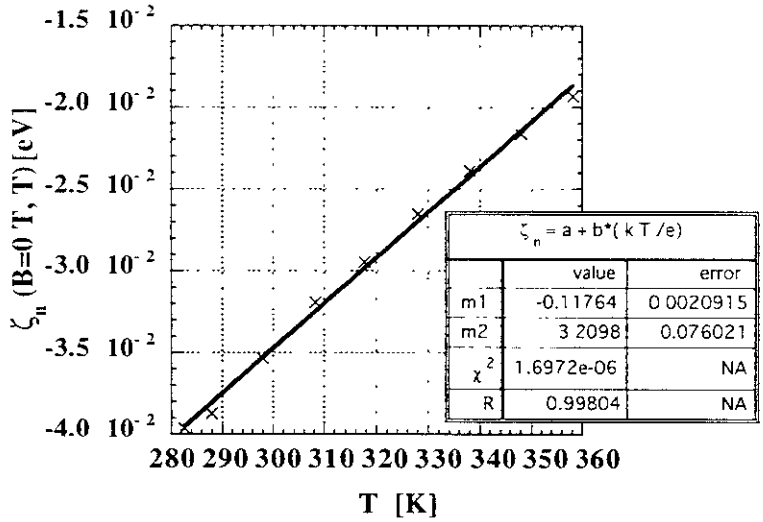

FIG. 10. Temperature dependence of the Fermi level. The experimental results are fitted by $\zeta_{\rm n} = -0.117 + 3.2\frac{kT}{|\epsilon|}$ [eV]. This equation denotes that $E_{\rm G} \approx 0.23$ [eV] and $m_{\rm p}/m_{\rm n} \approx 73$.

Recent Issues of NIFS Series

NIFS-503 E Segre and S Kida,
Late States of Incompressible 2D Decaying Vorticity Fields, Aug 1997

NIFS-504 S. Fujiwara and T. Sato,
Molecular Dynamics Simulation of Structural Formation of Short Polymer Chains, Aug. 1997

NIFS-505 S. Bazdenkov and T Sato
Low-Dimensional Model of Resistive Interchange Convection in Magnetized Plasmas; Sep 1997

NIFS-506 H Kitauchi and S Kida,
Intensification of Magnetic Field by Concentrate-and-Stretch of Magnetic Flux Lines; Sep. 1997

NIFS-507 R.L. Dewar,
Reduced form of MHD Lagrangian for Ballooning Modes, Sep 1997

NIFS-508 Y.-N Nejoh,
Dynamics of the Dust Charging on Electrostatic Waves in a Dusty Plasma with Trapped Electrons, Sep 1997

NIFS-509 E. Matsunaga, T Yabe and M. Tajima,
Baroclinic Vortex Generation by a Comet Shoemaker-Levy 9 Impact; Sep 1997

NIFS-510 C.C Hegna and N Nakajima,
On the Stability of Mercier and Ballooning Modes in Stellarator Configurations; Oct. 1997

NIFS-511 K. Orito and T Hatori,
Rotation and Oscillation of Nonlinear Dipole Vortex in the Drift-Unstable Plasma, Oct. 1997

NIFS-512 J Uramoto,
Clear Detection of Negative Pionlike Particles from H_2 Gas Discharge in Magnetic Field; Oct 1997

NIFS-513 T Shimozuma, M Sato, Y. Takita, S Ito, S. Kubo, H. Idei, K Ohkubo, T. Watari, T.S. Chu, K Felch, P. Cahalan and C M Loring, Jr,
The First Preliminary Experiments on an 84 GHz Gyrotron with a Single-Stage Depressed Collector; Oct. 1997

NIFS-514 T Shimozuma, S. Morimoto, M. Sato, Y Takita, S. Ito, S. Kubo, H. Idei, K. Ohkubo and T Watari,
A Forced Gas-Cooled Single-Disk Window Using Silicon Nitride Composite for High Power CW Millimeter Waves; Oct. 1997

NIFS-515 K Akaishi,
On the Solution of the Outgassing Equation for the Pump-down of an Unbaked Vacuum System; Oct 1997

NIFS-516 *Papers Presented at the 6th H-mode Workshop (Seeon, Germany)*; Oct. 1997

NIFS-517 John L Johnson,
The Quest for Fusion Energy; Oct. 1997

NIFS-518 J. Chen, N. Nakajima and M. Okamoto,
Shift-and-Inverse Lanczos Algorithm for Ideal MHD Stability Analysis, Nov. 1997

NIFS-519 M Yokoyama, N. Nakajima and M Okamoto,
Nonlinear Incompressible Poloidal Viscosity in L=2 Heliotron and Quasi-Symmetric Stellarators, Nov. 1997

NIFS-520 S. Kida and H Miura,
Identification and Analysis of Vortical Structures; Nov. 1997

NIFS-521 K. Ida, S Nishimura, T Minami, K Tanaka, S. Okamura, M. Osakabe, H. Idei, S Kubo, C. Takahashi and K. Matsuoka,
High Ion Temperature Mode in CHS Heliotron/torsatron Plasmas, Nov 1997

NIFS-522 M. Yokoyama, N. Nakajima and M. Okamoto,
Realization and Classification of Symmetric Stellarator Configurations through Plasma Boundary

Modulations; Dec. 1997

NIFS-523 H. Kitauchi,
Topological Structure of Magnetic Flux Lines Generated by Thermal Convection in a Rotating Spherical Shell; Dec. 1997

NIFS-524 T Ohkawa,
Tunneling Electron Trap; Dec. 1997

NIFS-525 K. Itoh, S.-I. Itoh, M Yagi, A. Fukuyama,
Solitary Radial Electric Field Structure in Tokamak Plasmas; Dec. 1997

NIFS-526 Andrey N. Lyakhov,
Alfven Instabilities in FRC Plasma; Dec 1997

NIFS-527 J. Uramoto,
Net Current Increment of negative Muonlike Particle Produced by the Electron and Positive Ion Bunch-method; Dec. 1997

NIFS-528 Andrey N. Lyakhov,
Comments on Electrostastic Drift Instabilities in Field Reversed Configuraiton; Dec. 1997

NIFS-529 J. Uramoto,
Pair Creation of Negative and Positive Pionlike (Muonlike) Particle by Interaction between an Electron Bunch and a Positive Ion Bunch; Dec. 1997

NIFS-530 J Uramoto,
Measuring Method of Decay Time of Negative Muonlike Particle by Beam Collector Applied RF Bias Voltage; Dec. 1997

NIFS-531 J. Uramoto,
Confirmation Method for Metal Plate Penetration of Low Energy Negative Pionlike or Muonlike Particle Beam under Positive Ions; Dec. 1997

NIFS-532 J. Uramoto,
Pair Creations of Negative and Positive Pionlike (Muonlike) Particle or K Mesonlike (Muonlike) Particle in H2 or D2 Gas Discharge in Magnetic Field; Dec. 1997

NIFS-533 S. Kawata, C. Boonmee, T. Teramoto, L. Drska, J. Limpouch, R. Liska, M. Sinor,
Computer-Assisted Particle-in-Cell Code Development; Dec. 1997

NIFS-534 Y. Matsukawa, T Suda, S. Ohnuki and C. Namba,
Microstructure and Mechanical Property of Neutron Irradiated TiNi Shape Memory Alloy; Jan. 1998

NIFS-535 A. Fujisawa, H. Iguchi, H. Idei, S. Kubo, K. Matsuoka, S. Okamura, K. Tanaka, T. Minami, S Ohdachi, S. Morita, H. Zushi, S. Lee, M. Osakabe, R. Akiyama, Y. Yoshimura, K. Toi, H. Sanuki, K. Itoh, A. Shimizu, S Takagi, A. Ejiri, C. Takahashi, M. Kojima, S. Hidekuma, K. Ida, S Nishimura, N. Inoue, R. Sakamoto, S.-I. Itoh, Y. Hamada, M. Fujiwara,
Discovery of Electric Pulsation in a Toroidal Helical Plasma; Jan 1998

NIFS-536 Lj R. Hadzievski, M.M. Skoric, M. Kono and T. Sato,
Simulation of Weak and Strong Langmuir Collapse Regimes, Jan. 1998

NIFS-537 H. Sugama, W. Horton,
Nonlinear Electromagnetic Gyrokinetic Equation for Plasmas with Large Mean Flows; Feb. 1998

NIFS-538 H. Iguchi, T.P. Crowley, A. Fujisawa, S. Lee, K. Tanaka, T. Minami, S. Nishimura, K. Ida, R. Akiyama, Y. Hamada, H., Idei. M. Isobe, M. Kojima, S. Kubo, S. Morita, S. Ohdachi, S. Okamura, M. Osakabe, K. Matsuoka, C. Takahashi and K. Toi,
Space Potential Fluctuations during MHD Activities in the Compact Helical System (CHS); Feb. 1998

NIFS-539 Takashi Yabe and Yan Zhang,
Effect of Ambient Gas on Three-Dimensional Breakup in Coronet Formation Process; Feb. 1998

NIFS-540 H. Nakamura, K. Ikeda and S. Yamaguchi,
Transport Coefficients of InSb in a Strong Magnetic Field; Feb. 1998